Temperature-dependency performance of InGaAsP semiconductor laser amplifiers

R. M. Ibrahim[a], I. B. Karomi[a,*], O. F. Ameen[a], M. S. Al-Ghamdi[b]
[a]*University of Mosul, College of Education for Pure Science Mosul, Iraq 41002*
[b]*Department of Physics, Faculty of Science, King Abdulaziz University, P.O. Box 80203, Jeddah 21589, Saudi Arabia*

We report a theoretical analysis on the influence of operation temperature on the static and dynamic properties of an InP/InGaAsP semiconductor Laser amplifier (SLA). We use a numerical wideband steady-state model and numerical algorithm, to study the (I-P) curves, gain bandwidth, noise figure, outpout noise power and outpout OSNR in a range between -20 °C and 100 °C. InP/InGaAsP SLA exhibited a thershold curent as low as 55mA at 100 °C and the characteristic temperature (T_0) of the SLA was found to be 142.8 ^{0}C, which confirms the high temperature operation of the device. Moreover, the results show that InP/InGaAsP SLA can cover 3dB operating at signal wavelengths between 1.54μm and 1.58μm with gains of up to 25dB at -20 ^{0}C. This peak slightly decreases with temperature. Furthermore, a high out power saturation of 7 dB was exhabited at -20 °C and a low noise figure of around 2.8 dB was achieved in the deviece. Finally, our model shows the elegant performance of InGaAsP/InP SLA in the range between -20 °C and 100 °C, which makes it a promising candidate for integrated photonics.

(Received November 26, 2020; Accepted April 3, 2021)

Keywords: Steady-state models, Semiconductor laser, SOA, Dynamic characteristics

1. Introduction

Semiconductor laser amplifiers (SLAs) or semiconductor optical amplifiers (SOAs) are vital elements in integrated optoelectronics and optical communications, such as optical switches [1], optical signal processing [2], pulse shaping [3], wavelength converters [4], clock recovery [5], wavelength-division-multiplexing (WDM) [6], and coherent optical communication [7]. This is mostly due to their broad bandwidth with high bit rate transmission [8], low noise figure [9], wide wavelength range for input and output signals [10], low chirp [11], insensitivity to the polarization [12], high nonlinearity [13] and lower cost [14]. SOAs are optoelectronic devices (e.g., semiconductor lasers) that amplify light; however, they amplify light in a single pass without optical cavity (see Fig. 1).

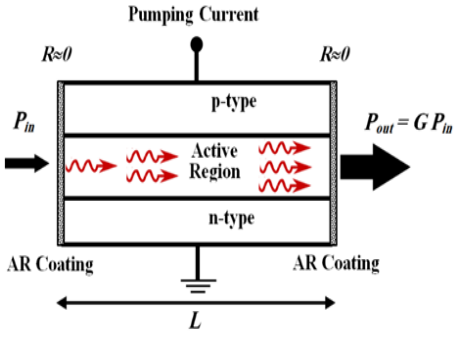

Fig. 1. Amplification process in a traveling-wave SOA.

* Corresponding author: ivanbahnam@uomosul.edu.iq

Understanding the operation and preference of SOAs is vital in modern optical communication systems. Consequently, many experimental and theoretical studies have attempted to understand the physics and operation of these materials; and hence have aimed to design an optimum and efficient SOA element. Most of these studies have focused on the effect of the operating conditions (i.e., bias current, modulation frequency, etc.) on the optical and dynamic properties of SOAs [15, 16, 17, 18]. Furthermore, the noise figure, outpout noise power and outpout of SOA has been accurately studied. For example, in [19] the noise level was significantly reduced by co-propagating the injection, from both the theoretical and experimental point of view. In [20], a bulk InP/InGaAsP SOA was described using a wideband steady-state model with different geometrical parameters. In [21], a high pumped current was used at moderate input signal power to reduce the noise in long SOAs. In [22], a wideband model was applied to describe the operation of strained MQW-SOA under wide range of bias currents. In [23], the effect of temperature up to 55 ^{0}C on the operation of InP and GaAs SOAs material was experimentally reported, and it was shown that GaAs SOA is less sensitive to the temperature with a less ASE level. In [24], InAs QD SOA was experimentally demonstrated for a temperature up to 100 °C. To the best of our knowledge, the effect of operation temperature on SOA characterization has not yet been theoretically analyzed. Moreover, it is possible that the temperature of the device changes under operation, by means of both self-heating and external mechanisms such as the temperature of the surrounding environment. Therefore, the intention of this article is to study an InP/InGaAsP wideband SOA through numerical simulations based on a wideband steady-state model in a temperature range of between -20 °C and 100 °C.

2. Amplifier structure and numerical model

The sample under discussion is a bulk heterostructure p-i-n junction. To increase optical confinement and electrical confinement in the active region, the lower bandgap intrinsic region of 1.55μm InP/InGaAsP (see Fig. 2). Current is pumped into the active region to produce a high population of carriers. The carrier density should overcome the transparency carrier density to get an optical gain in the material, and hence amplify optical signals through the stimulated emission process. During operation as an optical amplifier, light is coupled into the waveguide at Z=0. The light is amplified as it goes through the waveguide. Eventually, at Z=L, the out pout power is considerably higher than at Z=0.

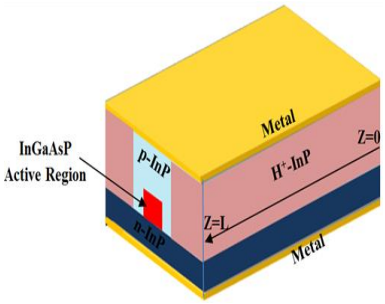

Fig. 2. SOA schematic.

The SOA numerical model that is used in this study is built on a set of differential equations that demonstrate the dynamicity of carrier and photon flux rates described in [20, 21]. The traveling-wave equations for the signal fields can be described as:

$$\frac{dE_{S_k}^{\pm}(z)}{dz} = \left[\pm jB_k \pm {}^1\!/_2\left(\Gamma\, g_m\left(v_k, N(z)\right) - \alpha\right)\right] dE_{S_k}^{\pm}(z) \tag{1}$$

Here, $dE_{S_k}^{\pm}(z)$ is a complex traveling wave, in both z-direction; (β_k) is the coefficient of propagation; (α) is the material loss; $g_m(v_k, n)$ is the material gain coefficient; and Γ is the optical confinement factor. The traveling-wave equations for the spontaneous emission are given by [20]:

$$\frac{dN_j^{\pm}(z)}{dz} = \pm\left[\left(\Gamma\, g_m\left(v_j, N(z)\right) - \alpha\right)\right] N_j^{\pm}(z) + R_{sp}\left(v_j, N(z)\right) \quad (2)$$

Here, $N^{\pm}_{\mathrm{j}}$ is the spontaneous emission rate in both z-direction; and R_{sp} is the emission noise coupled into N^{+}_{j} and N^{-}_{j}. The carrier density positive z-direction complies the rate equation and can be written as [20]:

$$\frac{dN(z)}{dt} = \frac{I}{edLW} - R\big(N(z)\big) - \frac{\Gamma}{dw}\left\{\sum_{k=1}^{N_s} g_m(v_k, N(z))(N_{s_k}^{+}(z) + (N_{s_k}^{-}(z)\right\} - \left\{\sum_{j=1}^{N_m-1} g_m\left(v_j, N(z)\right) K_j(N_j^{+}(z) + (N_j^{-}(z)\right\} \quad (3)$$

Here, I is the current; R is the recombination rate; e is elementary charge; Ns is the number of signals injected in the SOA; $N_{s_k}^{+}$ is the photon rate in the positive direction; and $N_{s_k}^{-}$ is the photon rate in the opposite direction. Originally, equations 1 to 3 can be solved numerically. The material gain can be calculated, as follows [20]:

$$g_m(v,n,t) = \left(\frac{c^2}{4\sqrt{2}\,\pi^{3/2}\, n_T^2\, t\, v^2}\right).\left(\frac{2m_e\, m_{hh}}{h\;\; 2\pi.(m_e + m_{hh})}\right)^{3/2} .\sqrt{v - \frac{E_g(n)}{h}}\;[f_c(v) - f_V(v)] \quad (4)$$

Here, c is the speed of light; h is the Planck constant; and τ is the radiative recombination lifetime. The noise figure (NF) and the optical signal to noise ratio (OSNR) can be numerically calculated from the model, as introduced in [21]. Finally, the other physical factors that we have used in the modeling are defined in Table 1.

Table 1. Alcatel SOA device parameters used for simulations.

Symbol	Descreption	Value	Units
L	Active area length	700	µm
$\mathcal{W}$	Active area width	0.4	µm
d	Active area thickness	0.4	µm
Γ	Optical confinement factor	0.45	----
A	Linear recombination coefficient	36 x10^{7}	1/s
B	Recombination coefficient	5.6×10^{-16}	m^3s^{-1}
C	Auger coefficient	3×10-41	m^6s^{-1}
v_g	Group velocity	75 x 10^{6}	m/s
n_t	Linear radiative recombination coefficient	1.4×10^{24}	m^{-3}
m_e	Effective mass of electron in the conduction band	4.1×10^{-32}	kg
m_{hh}	Effective mass of a hh in the valence band	4.19×10^{-31}	kg
m_{hl}	Effective mass of a lh in the valence band	5.06×10^{-32}	kg
dn_r	Differential of active refractive index regarding to carrier density	-1.8×10^{-26}	m^{-3}
n_{eq}	Equivalent effective refractive index at zero carrier density	3.22	-----
dn_{eq}	Differential of equivalent refractive index at zero carrier density	-1.8×10^{-26}	m^{-3}
k_q	Bandgap shrinkage constant	9×10^{-11}	eVm
Eg_0	Bandgap energy with no injected carrier	0.77725	eV
K_o	Carrier independent absorption loss coefficient	6200	m^{-1}
K_1	Carrier dependent absorption loss coefficient	7.5×10^{-21}	m^2
$\mathcal{Y}$	Composition of arsenide in the active region	0.892	-----

3. Result and dissuasion

3.1. Optical characteristics of SOA

The output optical power against driven current is plotted in Fig. 3 at different operation temperatures for the SOA, namely -20, 20, 60 and 100 ^{0}C. The input signal power is taken as -20dB and the wavelength signal is kept at 1550 nm. The threshold current (I_{th}) of the device is approximately 35 mA at 20 ^{0}C, which is a convenient value in comparison with some recent results for modern semiconductor materials [25, 26]. Furthermore, the threshold current increases when temperature is increased (the plot of Ln(I_{th}) versus temperature is pictured in Fig. 4). We calculate the characteristic temperature (To) as 142.8 ^{0}C, which is harmonic with the results in [27]. Furthermore, the sample showed a high temperature operation, which makes it a reliable device for optical network communication.

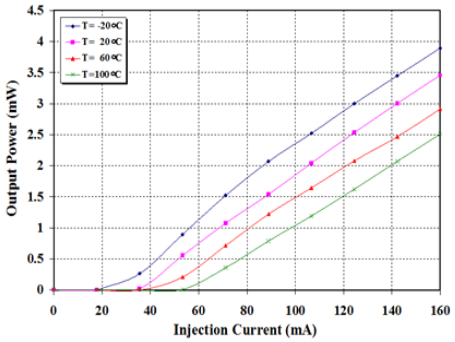

Fig. 3. Power-current curves at 20, 20, 60 and 100 ^{o}C, input signal power is -20dB and signal wavelength is 1550 nm.

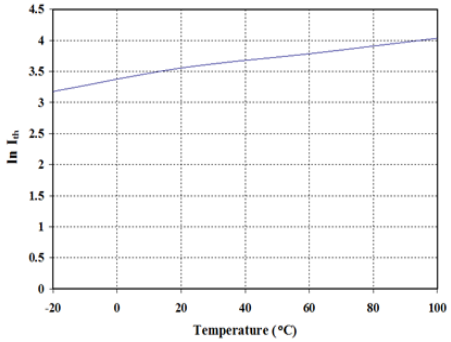

Fig. 4. The relationship between In(I_{th}) and temperature.

3.2. Static characteristics of the SOA

Fig. 5 shows the simulated gain spectra for SOA at different temperatures, and with a fixed driven current (140 mA) and input signal power (-20 dB). The value of the peak gain reduces and shifts towards longer wavelengths when temperature is increased. Moreover, the gain bandwidth of the ASO also decreases when temperature increases. Fig. 6 shows fiber-to-fiber gain against output power at fixed driven current (140mA), input signal wavelength (1550 nm), and at different temperatures. Fig. 7 shows fiber-to-fiber gain against input power at fixed driven current (140mA), fixed input signal wavelength (1550 nm), and at different temperatures. Saturation power versus temperature for both input and output power cases is plotted in Fig. 8. The 3dB gain for both input power and output power decreases with increasing temperature. The temperature coefficient is plotted versus input power in Fig. 9. It is found that by increasing the input power signal of the SOA, the effect of temperature on the SOA decreases. At a signal above -10dB, the temperature coefficient does not change with input power signal. Gain level above 28 dB was

achieved at -20 °C, which reduce to 25 dB at 100 °C. The result at -20 °C shows a high power saturation range, which mantains the linear working region and hence gives a higher dynamic range.

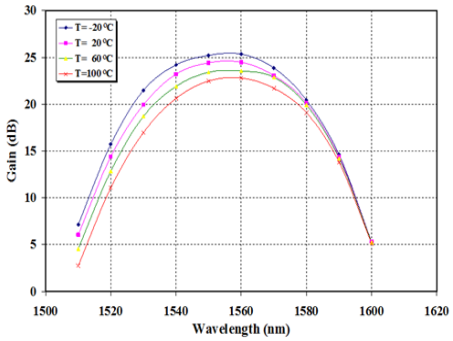

Fig. 5. Gain spectra for SOA AT 20, 20, 60 AND 100°c, Signal power – 20dB and Injection curret 140mA.

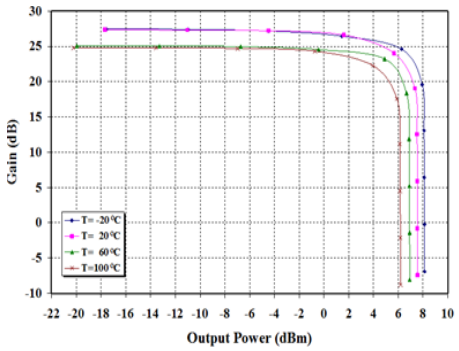

Fig. 6. Fiber-to-fiber gain versus output power at 20, 20, 60 and 100 and fixed wavelength of 1550 nm Injection curret 140 mA.

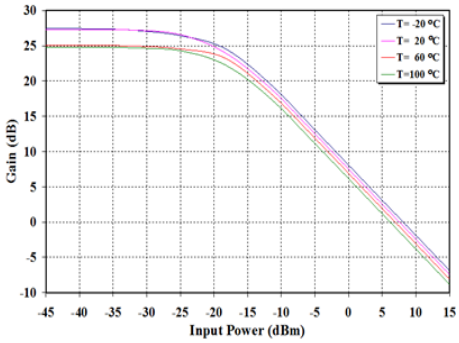

Fig. 7. Fiber-to-fiber gain versus input power at fixed driven current (140Ma) and fixed input signal wavelength (1550 nm).

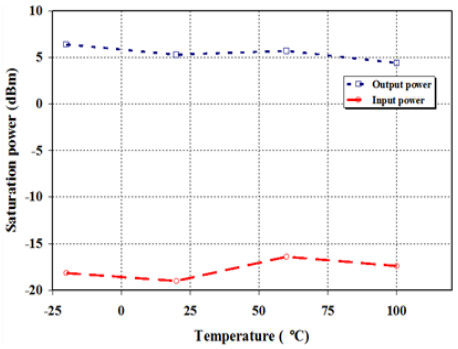

Fig. 8. Saturation power as a function of temperature for both input and output power cases.

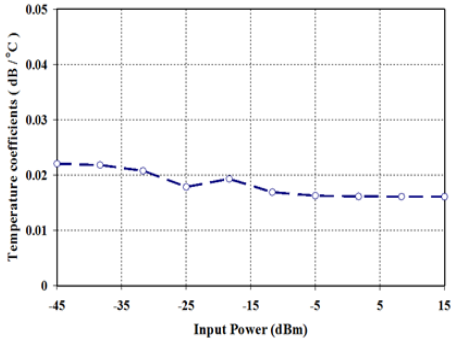

Fig. 9. Temperature coefficient versus input power.

3.3. Dynamic characteristics of the SOA

Fig. 10 represents the NF against the input power for different temperatures for SOA. At low input signal powers, the NF tends to constant values. At around -25 dB, the NF has the lowest value at 20 °C and the highest value at 60 °C. Then, at about -5 dB of the input signal power, NF has the lowest value at -20 °C and the highest value at 100 °C (which can be defined as threshold point). Therefore, the increase of input power raises the NF of the sample. Fig. 11 shows the noise power spectra of the SOA at different temperatures. It is obvious that by increasing the temperature, the noise power reduces. Moreover, the output noise power against input power is plotted in Fig. 12. The significant decreases of the output noise power occur in the range of input power of -20dB to -5dB. At -5dB, the entire range of temperatures that were studied show the same value of output noise power (around 42 dB). This is the linear working region for a SOA device with low noise power. Finally, the OSNR, which quantifies the degree of optical noise interference on optical signals, is also simulated in this study.

Fig. 13 reveals the output OSNR against the input power of the device at different temperatures. The results in Fig. 13 show that the SOA provides a high value of OSNR up to 58 dB at -20 ^{o}C in the linear working region. This could be an essential point for the DWDM networks that require operating above their OSNR limit to ensure error-free operation.

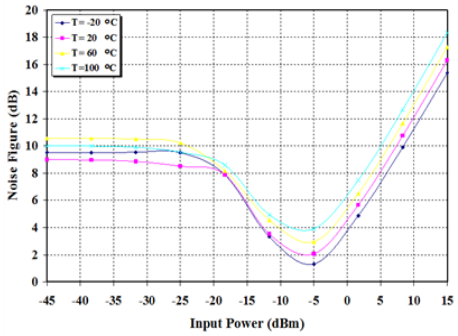

Fig. 10. Noise figure (NF) against the input power for various values of temperature for SOA wavelength is 1550 nm.

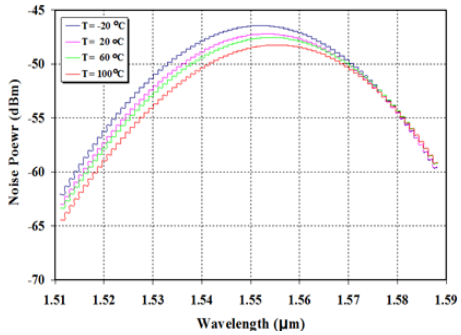

Fig. 11. The noise power spectra of the SOA at different temperatures.

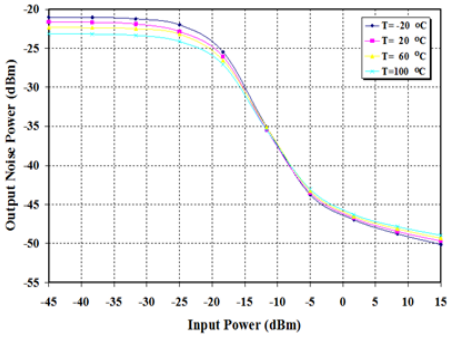

Fig. 12. Output noise power against input power. Wavelength is 1550 nm and injection current 140 mA.

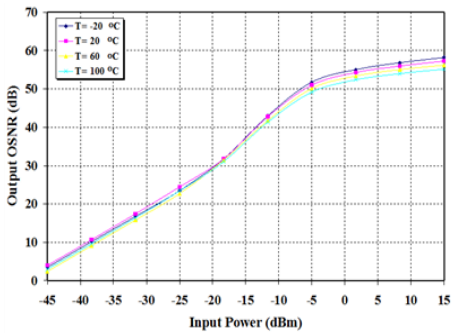

Fig. 13. Output OSNR as a function to the inout power at different temperatures. Wavelength is 1550 nm and injection current 140 mA.

4. Conclusion

We numerically solved the stady-state rate equations model of the InGaAsP/InP semiconductor Laser amplifier to study the operation profermance of this device at a range of tempertures (-20 to 100 ^{0}C). The sample showed a high temperature operation of the device with 55 mA thershold current at elevated temperature. Moreover, the results show the InP/InGaAsP SOA can amplify a wide signal wavelength range (1.54μm to1.58μm) with a peak gain of 25dB at -20 ^{0}C. Additionally, the introduced model of InGaAsP/InP SOA shows a wide linear working region for the SOA device with low noise power in the range between -20 °C and 100 °C. This makes it a promising candidate for integrated photonics. Finally, we hope that this work will be able to add to our understanding of the operation and performance of InP/InGaAsP SOAs.

References

[1] H. Ju, S. Zhang, H. Waardt, E. Tangdiongga, G. D. Khoe, H. J. S. Dorren. J. Opt. Express **13**, 942 (2005).
[2] U. Masashin, T. Munefumi, I. Ryo, N. Kohsuke, Proc SPIE **5246**, 263 (2003).
[3] H. Aghajanpour, V. Ahmadi, M. Razaghi. Optics & Laser Technology **41**, 654 (2009).
[4] M. Asghari, I.H. White, MemberJournal Of Lightwave Technology **15**, (1997).
[5] F. Wang, Y. Yu, Y. Zhang, X. Zhang, Journal of Lightwave Technology **30**, 1632 (2012).
[6] H. Nakano, S. Tsuji, S. Sasaki, K. Uomi, K. Yamashita, Journal of Lightwave Technology **11**, 612 (1993).
[7] H. Khaleghi, A. Sharaiha, T. Rampone, P. Morel, M. Guegan, IEEE Photonics Technology Letters **24**, 560 (2012).
[8] T. Ohtsuki, M. Matsuura, IEEE J. Photonics Technol. Lett. **30**, 459 (2018).
[9] A. Bilenca, G. Eisenstein, IEEE J. Quantum Electron **40**, 690 (2004).
[10] A. Bilenca, R. Alizon, V. Mikhelashhvili, D. Dahan, G. Eisenstein, R. Schwertberger, D. Gold, J. Reithmaier, A. Forchel, IEEE Photon. Technol. Lett. **15**, 563 (2003).
[11] A. V. Uskov, T. W. Berg, J. Mrk, IEEE J. Quantum Electron. **40**, 306 (2004).
[12] A. Farmani et al., Elsevior Opt. Laser Technol. **93**, 127 (2017).
[13] T. Matsumoto, K. Komatsu, G. Hosoya, H. Yashima, IET J. Electron. Lett. **54**, (2018), 580.
[14] T. Kiyama, M. Ekawa, M. Sugawara, K. Kawaguchi, H. Sudo, A. Kuramata, H. Ebe, Y. Arakawa, IEEE Photon. Technol. Lett. **17**, 1614 (2005).
[15] R. C. Figueiredo, N. S. Ribeiro, C. M. Gallep, E. Conforti, Opt. Commun. **336**, 153 (2015).
[16] J.-Y. Emery et al., Electronics Letters **33**, 1083 (1997).
[17] E. Udvary, Investigation of semiconductor optical amplifier direct modulation speed. 2014 16th International Conference on Transparent Optical Networks (ICTON), Graz, 1 (2014).
[18] A. Hamié, M. Hamze, J. L. Wei, A. Sharaiha, J. M. Tang, Opt. Express **19**, 25696 (2011).
[19] K. Obermann et al., IEEE Photonics Technology Letters **9**, 312 (1997).
[20] M. J. Connelly, IEEE Journal of Quantum Electronics **37**, 439 (2001).
[21] Y. Said, H. Rezig, A. Bouallegue, The Open Optics Journal **2**, 61 (2008).
[22] M. J. Connelly et al., Numerical Simulation of Optoelectronic Devices, 123 (2014).
[23] G. Giannoulis et al., IEEE International Conference on Electronics, Circuits, and Systems (ICECS), 677 (2015).
[24] O. Eyal, A. Willinger, S. Banyoudeh, F. Schanbel, V. Sichkovskyi, V. Mikhelashvili, J. P. Reithmaier, G. Eisenstein, Opt. Express **25**, 27262 (2017).
[25] Ivan Karomi, Peter M. Smowton, Samuel Shutts, Andrey B. Krysa, Richard Beanland, Opt. Express **23**, 27282 (2015).
[26] A. B. Krysa et al., J. Phys.: Conf. Ser. **740**, 012008 (2016)
[27] T. Higashi, T. Yamamoto, S. Ogita, M. Kobayashi, IEEE Journal of Selected Topics in Quantum Electronics **3**, 513 (1997).